



# JewelSuite AESubs Plug-In

---

*Quick Screening Subsidence Calculation*



## **Executive Summary**

The JewelSuite AESubs Plug-In provides easy to use subsidence calculations applicable on any Reservoir Model. Thanks to efficient integration in JewelSuite one can do a quick calculation of subsidence based on the reservoir depletion over time.

# Quick Screening Subsidence Calculation

---

## Table of Contents

Executive Summary .....	1
1 Copyright .....	3
2 References and Definitions .....	3
3 Introduction.....	3
4 AEsups calculation concept .....	4
4.1 AEsups: Forward Model Description.....	4
4.2 Integration to subsidence bowl due to compacting reservoir .....	8
4.3 Additional Output.....	9
4.4 Quality and robustness of the method .....	12
4.5 Area Sources: Evaluation of the influence functions .....	14
4.6 Accuracy of the Approximation with Area Sources .....	15
4.7 Limitations .....	19
5 JewelSuite integration.....	20

# Quick Screening Subsidence Calculation

---

## 1 Copyright

Copyright© 2009 JOA Oil & Gas BV. All Rights Reserved.

## 2 References and Definitions

S.L. Crouch and A.M. Starfield: Boundary Element Methods in Solid Mechanics: with Applications in Rock Mechanics and Geological Engineering: George Allen & Unwin, London, 1983

G. Fairweather and A. Karageorghis, The method of fundamental solutions for elliptic boundary value problems: Adv. Comp. Math. **9**, p. 69-95, (1998)

P.A. Fokker and B. Orlic, 2006: Semi-Analytic Modelling of Subsidence, Math. Geol, **38**, 565-589

R.D. Mindlin: Force at a point in the interior of a semi-infinite solids: Physics, no. **7**, p. 195-202. (1936)

Mulders, F.M.M. Modelling of Stress Development and Fault Slip in and around a Producing Gas Reservoir, PhD thesis, Delft University Press, 2003.

## 3 Introduction

The exploitation of reservoirs often has results connected to the geomechanical response of the subsurface. AEsSubs is a software tool that calculates geomechanical consequences of the reservoir exploitation, like subsidence and induced stresses and strains in the subsurface. In JewelSuite™ it is seamlessly integrated with the reservoir simulator.

## 4 AEsups calculation concept

The production of hydrocarbons from a reservoir is usually accompanied by a decrease of the reservoir fluid pressure. This pressure change influences the stress situation, and may induce compaction in the reservoir and surface subsidence. AEsups is a semi-analytical software tool to calculate such subsidence induced by the production of oil or gas.

The subsidence prediction tool AEsups can also output displacements, strains and stresses at other positions than the surface. The solution scheme that AEsups uses facilitates the calculation of this output: the solution is formulated in the form of analytic functions and output can thus be calculated at every point in the reservoir. However, for distances close to the reservoir, it is then not sufficient to take the reservoir pressure field as a collection of point sources of compaction, at positions centred in the grid blocks where the reservoir calculated the reservoir pressure. Therefore such required additional necessitates incorporating the areal extent of the reservoir grid blocks.

We will first briefly discuss the forward model capability of the software tool AEsups. Then the extension to area sources will be presented.

### 4.1 AEsups: Forward Model Description

AEsups employs a new modelling approach that combines elements of analytic and numerical approaches [P.A. Fokker and B. Orlic: Semi-Analytic Modelling of Subsidence, Math. Geol, 2006, in press]. The method combines a number of analytic functions that satisfy the elasticity equations in such a way that the boundary conditions are approximated. Such an approach makes the method more widely applicable than analytical approaches, while the calculation times are much smaller than for numerical (e.g. finite-element) simulators. It is typically 3 orders of magnitude faster than finite-element calculations and much more flexible in the sense that changes in the elasticity profile are easy to implement.

The semi-analytic method is similar to boundary-element methods [S.L. Crouch and A.M. Starfield: Boundary Element Methods in Solid Mechanics: with Applications in Rock Mechanics and Geological Engineering: George Allen & Unwin, London, 1983]. There are, however, a few differences. In the semi-analytic method singularities are distributed outside the domain, rather than on the boundaries of the domain. Then, the domain is split into multiple regions with different elastic properties. Finally, a least-squares approach is used to approximate the boundary conditions in a number of points rather than to honour them exactly, as it is the case in the conventional boundary element approach. The model can be viewed as belonging to the class of the method of fundamental solutions (MFS). MFS has been reviewed by Fairweather and Karageorghis [G. Fairweather and A. Karageorghis, The method of fundamental solutions for

## Quick Screening Subsidence Calculation

---

elliptic boundary value problems: Adv. Comp. Math. 9, p. 69-95, (1998)]. The quoted review paper describes the development of MFS over the previous three decades and presents several applications. The AEsSubs extension is the application to multiple layers of different elastic parameters and to viscoelasticity. Advantages of the approximate solution method of the elasticity equations are that relatively few boundary points and singularities are required, that it does not require elaborate discretization of the boundaries, and that the approximation of the solution and of derivatives can be evaluated directly at any given point. Implementation of the method is relatively easy and computation times are kept low. We present the elastic part of the model here; for the viscoelastic part we refer to our separate publication [P.A. Fokker and B. Orlic, 2006: Semi-Analytic Modelling of Subsidence, Math. Geol, **38**, 565-589].

The two equations that are relevant in the theory of linear elasticity are Hooke's law and the equilibrium equation. Hooke's law for linear elasticity, with inclusion of poro-elasticity, reads:

$$\sigma_{ij} = 2G\varepsilon_{ij} + \left[ \frac{2G}{1-2\nu} \varepsilon_{kk} - \alpha_{\text{Biot}} \Delta p \right] \delta_{ij} \quad \text{Eq. (1)}$$

where  $\sigma_{ij}$  is the stress tensor,  $\varepsilon_{ij}$  is the strain tensor,  $\Delta p$  is the change of pressure,  $G$  is the shear modulus,  $\nu$  is the Poisson's coefficient,  $\alpha_{\text{Biot}}$  is the Biot's constant and  $\delta_{ij}$  is the Kronecker delta.

Equation (1) is used further for the difference with the undisturbed state, which is possible due to its linearity. The equilibrium equation reads:

$$\partial_j \sigma_{ij} = 0 \quad \text{Eq. (2)}$$

The two equations are completed with the boundary and interface conditions. In media with discrete homogeneous elasticity parameters, which are the type of media treated in AEsSubs, the boundary conditions consist of vanishing tractions ( $\sigma_{i3}$ ) at the surface, and continuous tractions and displacements ( $u_i$ ) at interfaces:

$$\begin{aligned} \text{surface } (z = 0): \quad & \sigma_{i3} = 0 \\ \text{interfaces } (z = -d_1 \dots d_N): \quad & \begin{cases} \sigma_{i3} = \text{continuous} \\ u_i = \text{continuous} \end{cases} \end{aligned} \quad \text{Eq. (3)}$$

Solutions to the equations can be conveniently formulated using potential functions such as Galerkin stress functions. Galerkin stress functions, as defined in Mindlin's paper [R.D. Mindlin: Force at a point in the interior of a semi-infinite solids: Physics, no. 7, p. 195-202. (1936)] were used here, including a factor  $2G$  in the definition. The factor  $2G$  was included for

## Quick Screening Subsidence Calculation

---

convenient extrapolation to linear visco-elasticity. With a Galerkin vector  $\mathbf{F}$ , the displacements and the stresses are given by:

$$\begin{aligned} u_i &= 2[1-\nu]\nabla^2 F_i - \partial_i \partial_k F_k \\ \sigma_{ij} &= 2G\left\{\left(\nu\delta_{ij}\nabla^2 - \partial_i \partial_j\right)\partial_k F_k + [1-\nu]\nabla^2\left(\partial_i F_j + \partial_j F_i\right)\right\} \end{aligned} \quad \text{Eq. (4)}$$

In the absence of body forces, the Galerkin vector potential must satisfy the biharmonic equation:

$$\Delta^2 \mathbf{F} = 0 \quad \text{Eq. (5)}$$

AEsubs study makes use of solutions originating from nuclei of strain. A nucleus of strain refers to a well-defined singularity, for instance a force acting at a single point. A centre of compression, or a centre of compaction, is a nucleus of strain as well, and we use a distribution of these to represent the compacting reservoir. For a nucleus of strain located at  $(0,0,-d)$ , the following Galerkin stress functions are associated with a single force directed along the z-axis, a double force (i.e. a single-force dipole), a centre of compression, and a centre-of-compression dipole (also directed along the z-axis);  $\mathbf{k}$  is the unit vector in the z-direction;  $R$  is the distance to the nucleus,  $R = \sqrt{x^2 + y^2 + (z+d)^2}$ .

$$\begin{aligned} \mathbf{F}_{\text{singleforce}} &= \mathbf{k}AR & (a) \\ \mathbf{F}_{\text{doubleforce}} &= \mathbf{k}B \frac{z+d}{R} & (b) \\ \mathbf{F}_{\text{centreofcompression}} &= \mathbf{k}E \log(R+z+d) & (c) \\ \mathbf{F}_{\text{dipole}} &= \mathbf{k}H \frac{1}{R} & (d) \end{aligned} \quad \text{Eq. (6)}$$

The constants  $A$ ,  $B$ ,  $E$  and  $H$  are the strengths of the associated nuclei. For a volume  $dV$  in which the pressure is reduced by an amount  $dP$ , the strength  $E_0$  of the associated centre of compression is given by:

$$E_0 = -\alpha_{\text{Biot}} \frac{1-2\nu}{2G(1-\nu)} \frac{dVdp}{4\pi} = -c_m \frac{dVdp}{4\pi} \quad \text{Eq. (7)}$$

in which the compaction coefficient  $c_m$  has been expressed as a function of the Biot constant  $\alpha_{\text{Biot}}$ . The compaction coefficient indicates how much a reservoir with a large radius-to-thickness ratio would compact vertically per unit of reservoir thickness and per unit of pressure decrease (it has the dimension of  $[1/\text{Pa}]$ ).

# Quick Screening Subsidence Calculation

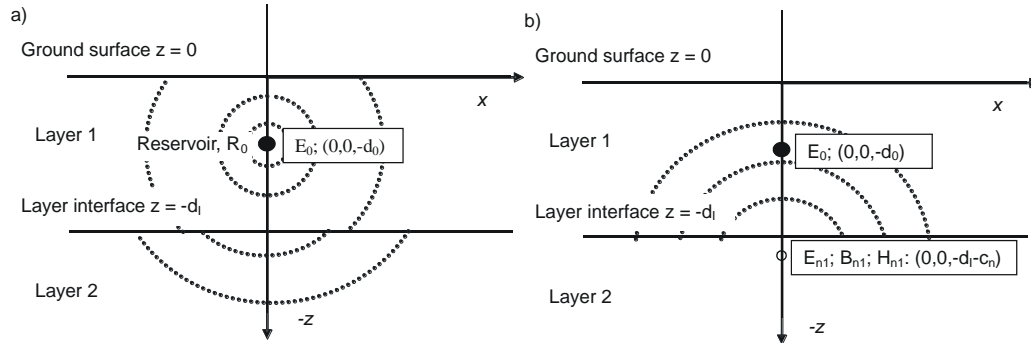


Figure 1 Schematic representation of the conceptual model.

- A. The centre of compression of strength  $E_0$ , located at  $(0,0,-d_0)$ , causes stress and strain fields that are discontinuous at the ground surface and at the interfaces between layers of different stiffness.
- B. With an auxiliary nucleus of strain  $E_{n1}$ ,  $B_{n1}$ , and  $H_{n1}$ , located in layer 2 at  $(0,0,-d_1-c_n)$ , additional stress and strain fields are generated in layer 1. These fields can be fine-tuned by adjusting the magnitude of the free strength parameters  $E_{n1}$ ,  $B_{n1}$ , and  $H_{n1}$ . Solution procedure makes use of several auxiliary nuclei located at different distances from the interface along the  $z$ -axis.

The method employed for solving the elasticity equations with the appropriate boundary conditions starts with the particular solution of the elasticity equations around a centre of compression, embedded in a homogeneous unlimited three-dimensional space, by using its Galerkin stress function [Eq. (6c)]. The full solution is applicable in the case of an infinite space with homogeneous properties. The problem at hand, however, involves a subsurface with an unconstrained ground surface and elasticity interfaces at the boundaries between the subsurface layers of different stiffness. The boundary conditions at the ground surface and at the interfaces in a layered subsurface are not honoured by the solution as defined by the centre-of-compression function alone: the fields derived from the stress functions depend on the shear modulus and the Poisson's ratio,  $G$  and  $\nu$ , respectively, and are therefore discontinuous across elasticity interfaces (Fig. 1A). The solution originating from the centre of compaction is therefore complemented by other solutions to the elasticity equations to correct for this. The centre of compression in the horizontally layered subsurface, however, does preserve rotational symmetry.

The additional solutions should be chosen in such a way to create additional discontinuities in the tractions and displacements at the layer interfaces and at the ground surface. These solutions should contain free parameters that can be used to fine-tune these discontinuities, so that they can be adjusted to let the resulting complete solution approximate the boundary conditions, viz. continuity of displacements and of tractions at interfaces and zero tractions at the ground surface. Because of the rotational symmetry of the problem, a cylindrical co-ordinate system can be used, and only the  $r$  and  $z$ -components need to be considered.

---

## Quick Screening Subsidence Calculation

---

The additional solutions are taken as originating from auxiliary nuclei of strain with rotational symmetry along the z-axis (Fig. 1B). A number of these nuclei are positioned at different distances from the interface along the z-axis. The field of a nucleus below the interface is applied only above the interface, and vice versa. In this way the singularity is kept outside the domain of application of the elastic field and the solution is a real solution to the elasticity equations in the full application domain. The piecewise application of additional fields induces additional discontinuities in the tractions and displacements. These can be influenced and optimised to meet the boundary conditions, by adjusting the strengths of the nuclei. The set-up of Figure 1 is applicable for a multi-layer subsurface: the fields of the auxiliary nuclei above an interface are applied at all positions below the interface with which it is connected, across the interfaces underneath, and similarly for nuclei below an interface of interest. Clearly, nuclei close to the interface act rather locally, whereas those further away affect a larger volume.

To determine the nuclei strengths, first a forward model is constructed with the deviation from the required boundary conditions as outcome. The strengths of the compaction source and of the auxiliary nuclei are input, the latter are unknowns. As this model is linear, a generalized inverse method straightforwardly results in the best estimate for the strengths of the auxiliary nuclei in the least-squares sense. In the least-squares approach, the number of points where the boundary conditions are evaluated exceeds the number of free strength parameters in the solutions of the elasticity equations.

### 4.2 Integration to subsidence bowl due to compacting reservoir

The solution obtained by using the method described above yields a subsidence bowl originating from a centre of compression, which is the mathematical representation of an amount of compaction concentrated at a single point. This subsidence bowl is rotationally symmetric. The solution is subsequently used as an influence function or Green function in conjunction with the reservoir data to arrive at the subsidence bowl for the whole reservoir that is compacting. Indicating the influence function for vertical displacement at the surface with  $g(r)$ , the reservoir height with  $H(x,y)$ , the pressure depletion with  $\delta p$  and the compaction coefficient with  $c_m$ , we have:

$$u_3(x, y) = c_m \int_{\text{reservoir}} H(x', y') \cdot \delta p(x', y') \cdot g\left(\sqrt{(x - x')^2 + (y - y')^2}\right) dx' dy' \quad \text{Eq. (8)}$$

For a reservoir with large area compared to its height  $H$ , the compaction (which in this case would be purely vertical) would amount to  $c_m \cdot H \cdot \delta p$ . The integration breaks the rotational symmetry: a reservoir grid of arbitrary outline can be used.

---

## Quick Screening Subsidence Calculation

---

If the reservoir pressures are available from reservoir simulations on discretized models, first the product  $\delta V \cdot \delta P$  for the strength of the nucleus is calculated for the centroid of each grid block in the reservoir. Then the integral of Eq. (8) is replaced by a summation over all the active grid blocks in the reservoir:

$$u_3(x, y) = c_m \sum_i \delta V_i \cdot \delta p_i \cdot g\left(\sqrt{(x - x_i)^2 + (y - y_i)^2}\right) \quad \text{Eq. (9)}$$

The approximation of the influence function of a grid cell by the influence function of a centre of compression in its centre is appropriate as long as the ground surface is far enough away, i.e. the depth is more than 10 times the typical dimension of the grid block. The mismatch is then typically less than 1%. For shallow reservoirs like depleting aquifers, the influence function in Eq. (9) needs to be replaced by a volume integral of the influence function over the grid block. This is the topic of the next Chapter.

The method is applicable to linear theories because it relies on the superposition principle for solutions of the elasticity equations. It can be extended to other linear elastic systems like transverse isotropy or orthotropy, but not to non-linear theories as power-law creep with a coefficient different from unity.

### 4.3 Additional Output

Additional output can be generated to evaluate stresses, strains and displacements as induced by the compacting field in points that the user is interested in. The stresses calculated with AEsups are the stresses additional to the stresses already in place. The actual total stress is the sum of the original stress and the stress induced by the compacting field.

For the calculation of the stresses and displacements on the selected points, roughly the same procedure is followed as for the calculation of the surface subsidence bowl. The main difference is that no general influence function is constructed but the influence of every nucleus on every point is evaluated explicitly. This is necessary because the points may have different depth.

For all the points the six independent components of the stress tensor, the six components of the strain tensor, and the three displacement components are evaluated. From the stress tensor  $\sigma$ , the normal stress and the shear stress in the user-defined plane are evaluated. When the normalized vector normal to the plane is called  $\mathbf{n}$ , the total stress in this plane (i.e. the force per unit area) is calculated as  $\mathbf{f} = \sigma \mathbf{n}$ ; the normal stress is then  $\sigma_n = \mathbf{f} \cdot \mathbf{n}$  and the absolute value of the shear stress is  $\tau = \sqrt{f^2 - \sigma_n^2}$ .

The final stress following depletion of an oil or gas field, or, for that matter its pressurization, consists of the initial in-situ stress and the induced stress. Therefore the initial stress is an additional input. Stress in three dimensions can be represented with regard to any orthogonal co-

---

## Quick Screening Subsidence Calculation

---

ordinate system as a symmetrical matrix with 3 rows and 3 columns. With a suitable choice of the co-ordinate system orientation, the stress matrix can be transferred to a diagonal matrix with the three principal stresses on the diagonal. In most cases, the orientation of the largest principal stress is vertical. Therefore we have limited the input stress field to stresses with one vertical principal stress. The remaining principal orientations are then horizontal and the full stress tensor is characterized by the minimum, the medium, and the maximum in-situ stress values and the orientation of the medium in-situ stress with regard to North.

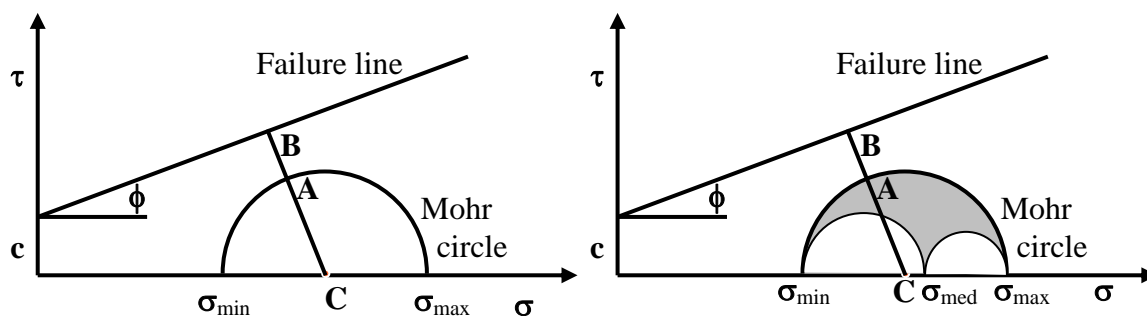
The setup of AEsups is based on a layered subsurface. For each layer the stress at its top (3 principal stresses and 1 orientation) and a stress gradient (for the 3 principal stresses) can be formulated. The same initial stress is assumed to be present at all locations of the same depth. From this input the total stress tensor can be easily computed in every location in the subsurface.

In practice the stress is often given in terms of a stress gradient only. We have therefore added the possibility to calculate the stress with a value at the surface and values for the gradients in the different layers, under the assumption that at the interfaces the stress is continuous.

Failure is usually calculated as a function of the effective stress. The effective stress is the difference between the total stress and the pore pressure. We have thus also added the pore pressure as an input field. As with the stress, it is characterized by a value at the top of each layer and a gradient. With the calculation option from the gradients, the pore pressure is also calculated.

The most commonly used failure criterion is the Mohr-Coulomb criterion. This report will not go into large detail describing it, but some notions must be mentioned.

The Mohr circle is a graphical representation of the effective stress situation in the subsurface. In 2D, all the combinations of normal and shear stress ( $\sigma$  and  $\tau$ ) lie on a circle in the  $(\sigma, \tau)$  plane that connects the minimum and the maximum principal stresses on the  $\sigma$ -axis. In 3D the situation is slightly more complicated but a Mohr circle can still be constructed for every plane. The Mohr-Coulomb failure criterion states that the material fails once part of the Mohr circle falls above the failure line, which is characterized by  $\tau = c + \sigma \sin\phi$ . The constant  $c$  is the cohesion; the angle  $\phi$  is called the friction angle. This is visualized in Fig. 1.



## Quick Screening Subsidence Calculation

Figure 1. Graphical representation of the effective stress in the Mohr circle and of the Mohr-Coulomb failure line, in 2D (top) and 3D (bottom).

A measure indicating how far the material is from failure is the proximity of the Mohr circle to the failure line [Mulders 2003]. This proximity is quantified in the mobilized shear capacity, defined as the ratio of distances  $AC / BC$  (Fig. 1). When the maximum ratio of 1 is reached, the material will fail. When the risk on reactivation of a plane must be assessed, the traction on that plane is calculated and plotted in the  $(\sigma, \tau)$  plane, and a line perpendicular to the failure line is constructed to calculate this ratio. A more general problem is when the risk on failure in a point must be assessed irrespective of the plane of failure. In that case, the maximum and minimum principal stresses in that point are calculated, and the ratio  $AC / BC$  is calculated with  $AC$  the radius of the circle  $\frac{1}{2}[\sigma_{\max} - \sigma_{\min}]$  and  $BC$  the distance from point  $C = (\frac{1}{2}[\sigma_{\min} + \sigma_{\max}], 0)$  to the failure line.

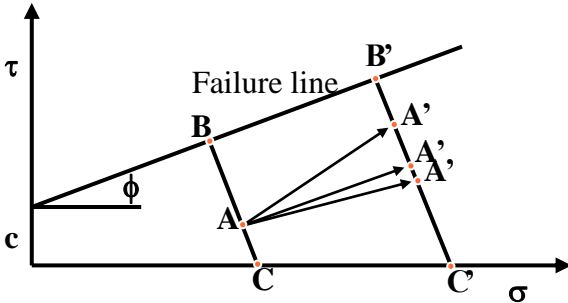


Figure 2. Visualization of the stress path,  $AA'$ . While the mobilized shear capacity increases for all three paths ( $A'C' / B'C' > AC/BC$ ), the stress path of the lower two arrows is non-critical:  $A'B' \geq AB$  for the lower two arrows.

The proximity of the stress to failure is not the only way of considering the risk to, for instance, fault reactivation. A different approach is to assess the criticality of the stress path. The stress path is the development of the effective stress due to the depletion or pressurization of the reservoir. It is called critical if the effective stress moves toward the failure line, and non-critical otherwise. The criticality of the stress path is easily quantified by calculating the change in distance  $AB$  before and after depletion or pressurization. We can make the same distinction between reactivation of an existing fault, where the stress needs to be evaluated on a predefined plane only, and failure in a point irrespective of the plane of failure. In some cases, an increase in mobilized shear capacity does not imply a critical stress path. Such a situation is visualized in Fig. 2.

An essential parameter in seismic inversion is the seismic velocity. It provides the link between the travel times and the depths of the seismic scatterers. In 4D seismics, consecutive campaigns are carried out with the goal to learn from the differences in seismic response. Depletion or pressurization of a reservoir change the seismic velocity considerably, and also influence the refractive properties of interfaces. However, the change in strain in regions where the pressure is

---

## Quick Screening Subsidence Calculation

---

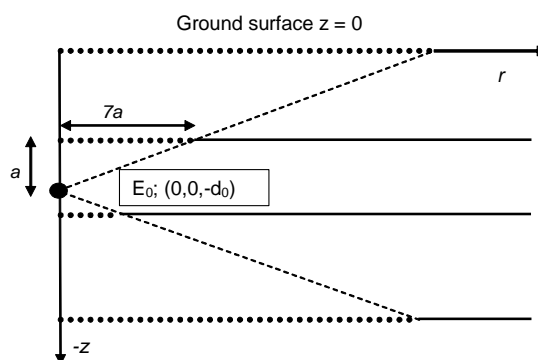
not affected also has a bearing on the velocity. The vertical strain is in particular important. Correlations are available between changes in the vertical strain and the seismic velocity. Therefore it is important to also have an indication of the change in strain around the reservoir. We have extended the AEsSubs output on user-defined lines and planes with the full strain tensor. For completeness, we here list the strain components for the different nuclei of strain used in AEsSubs and the expressions resulting when they are integrated over an areal source..

### 4.4 Quality and robustness of the method

The quality and robustness of the approximation were tested in order to determine the optimal way of determination of the strengths of the auxiliary sources. Further tests were performed to optimize the number, position and type of the auxiliary nuclei required to use in the model for subsidence prediction.

A first qualitative assessment of the quality of the approximation could be obtained by judging the curves representing the tractions and the displacements at the boundaries and the interfaces. These should be physically sensible: asymptotically approaching zero at infinity; and having the maximum value (or the maximum derivative) at the origin.

A more quantitative judgement of the quality of the approximation was obtained by means of the summed squared deviation from the boundary and interface conditions: the zero tractions at the ground surface, and the zero difference of tractions and displacements at the layer interfaces. Various representations of summed squared deviations were implemented and tested. The most robust scheme was achieved when the strengths of the nuclei were adjusted to minimize the summed squared deviations on a number of equidistant points. For each interface, the equidistant points should extend in the radial direction, starting from the position right on top of the compaction source ( $E_0$ ), up to 5 to 10 times the vertical distance to it (Fig. 2). A value of 7 has been implemented in the code.



---

## Quick Screening Subsidence Calculation

---

Figure 2 Distribution of the equidistant points at which the interface conditions are evaluated. The distribution extends to 7 times the vertical distance to the compacting source  $E_0$ .

The robustness of the approximation was assessed by testing the effect of different elasticity profiles. This was done by judging the quality versus the variation in profile, but also by assessing the variation in the resulting maximum level of subsidence and the variation in the volume of the subsidence bowl for a given centre of compression.

The sensitivities to the number of nuclei showed that a reasonable subsidence profile was usually obtained with 8 nuclei for each side of each interface. For elasticity profiles with relatively large contrast in stiffness, i.e. changes in elasticity between adjacent layers larger than a factor of 2, more nuclei were required. 8 to 10 pairs of nuclei around each interface were usually sufficient to obtain accurate results: using 10 pairs instead of 8 often resulted in a fit of better quality, but did not change the resulting subsidence more than 1 – 2 % in terms of depth and 2 – 5 % in terms of volume.

The sensitivities showed that it was absolutely necessary to position the nuclei around the associated interface at distances of the same order of magnitude as the vertical distance of this interface to the original source (i.e. the compacting reservoir). Logarithmically spaced nuclei at distances to the interface of 0.25 to 13 times the distance to the compaction source ( $E_0$ ) usually gave optimal result. In specific cases this logarithmic pattern of the auxiliary nuclei could be improved, and in some cases it was not possible to achieve an acceptable quality. Such instabilities in the model were usually associated with large contrasts in elastic moduli (larger than a factor 10), large differences in layer thicknesses, or a short distance between compacting source and one of the interfaces. It is therefore advisable to always check the quality of the approximation before proceeding with the integration exercise.

The sensitivities to the type of the auxiliary nuclei of strain were tested by using different combinations of nuclei types [Eq. 6]. The best results were achieved with combinations of centres of compression, double forces and doublets of centres of compression in the z-direction [Eqs. (6b), (6c), and (6d)]. These types of nuclei were also used by Mindlin to derive the analytical expression for a homogeneous half-space. Including single forces [Eq. (6a)] gave worse results as their fields damp out more slowly than the fields of a centre of compression. Including the dipole [Eq. (6d)] was not strictly necessary but facilitated the same quality of approximation with fewer nuclei. The combination of these three types of nuclei provided sufficient flexibility for our type of problems with circular symmetry around the z-axis. The associated equation for the stresses and the displacements in, e.g., the uppermost layer reads:

## Quick Screening Subsidence Calculation

---

$$\begin{aligned}\sigma_{ij} &= \sigma_{ij}(E_0) + \\ &\quad \sum_m [\sigma_{ij}(E_m) + \sigma_{ij}(B_m) + \sigma_{ij}(H_m)] + \\ &\quad \sum_{n1} [\sigma_{ij}(E_{n1}) + \sigma_{ij}(B_{n1}) + \sigma_{ij}(H_{n1})] \\ u_i &= u_i(E_0) + \\ &\quad \sum_m [u_i(E_m) + u_i(B_m) + u_i(H_m)] + \\ &\quad \sum_{n1} [u_i(E_{n1}) + u_i(B_{n1}) + u_i(H_{n1})]\end{aligned}\tag{Eq. (10)}$$

where the summations over  $m$  are over nuclei above the surface and the summations over  $n1$  are over nuclei below the first interface.

### 4.5 Area Sources: Evaluation of the influence functions

The problem with the use of point sources for the calculation of stresses and displacements was already indicated in the end of the previous Chapter. Point sources do not suffice when the position where the calculation is required is close to that point. The quantification when a point is close in this sense relates to the size of the grid block. The approximation with point sources results in an error typically less than 1% when the distance is larger than 10 times the largest dimension of the grid block. The dimensions of the grid block thus need to be taken into account explicitly when subsidence is calculated above reservoirs for which the grid block size is larger than 10% of the depth. The grid block dimensions must also be taken into account when stresses and displacements need to be calculated in arbitrary points.

For volume sources, the influence function for the vertical displacement in Eq. (9) needs to be replaced by a volume integral. A similar argument holds for the other displacements and for the stresses. We have chosen not to integrate over the height of a grid block. The volume integrals are thus reduced to area integrals. The next Section will support the validity of this approximation.

The subsidence bowl is the displacement in the vertical direction at the surface as a function of the position in  $x$  and  $y$ . All the points where the displacement is calculated are thus at the same vertical distance from the nuclei that constitute the solution of the source nuclei at the reservoir depth. Therefore, when all the grid blocks have the same dimensions, an influence function can be constructed once for a grid block of that size, to be used in the integration over all the grid blocks. This procedure saves a lot of computing time and has therefore been implemented in the code. When the code needs to be extended with grid blocks of variable size, the integration over all the grid blocks requires evaluation of the influence function with due account of all the nuclei for every single block.

## Quick Screening Subsidence Calculation

---

We take as an example the normal stress in the x-direction originating from a doublet. From Eq. (4) we have for a point source at position  $(x_0, y_0, 0)$  in the horizontal plane with  $z_0 = 0$

$$\begin{aligned}
 R &= \sqrt{(x-x_0)^2 + (y-y_0)^2 + z^2} \\
 F_3 &= H \frac{1}{R} \\
 \sigma_{11} &= 2G \left\{ \left( \nabla^2 - \partial_1 \partial_1 \right) \partial_3 F_3 \right\} \\
 &= 2GH \left\{ \frac{3z}{R^7} \left[ 4(x-x_0)^2 - (y-y_0)^2 - z^2 \right] \right\}
 \end{aligned} \tag{Eq. (11)}$$

and the effect of a homogeneous distribution of doublets over a rectangular area in the horizontal plane gives

$$\begin{aligned}
 \sigma_{11} &= 2GH \int_{x_1}^{x_2} \int_{y_1}^{y_2} \frac{3z}{R^7} \left[ 4(x-x_0)^2 - (y-y_0)^2 - z^2 \right] dy dx \\
 &= 2GH \left\{ P[\sigma_{11}^H](x_2-x_0, y_2-y_0) - P[\sigma_{11}^H](x_2-x_0, y_1-y_0) \right. \\
 &\quad \left. - P[\sigma_{11}^H](x_1-x_0, y_2-y_0) + P[\sigma_{11}^H](x_1-x_0, y_1-y_0) \right\}
 \end{aligned} \tag{Eq. (12)}$$

in which  $P[\sigma_{11}^H]$  is the primitive function of the integrand:

$$\begin{aligned}
 \frac{\partial^2}{\partial x' \partial y'} P[\sigma_{11}^H](x', y') &= \frac{3z}{R^7} [4x'^2 - y'^2 - z^2] \\
 P[\sigma_{11}^H](x', y') &= \frac{-x' y' z}{(x'^2 + z^2)^2 R^3} (3R^2 - y'^2)
 \end{aligned} \tag{Eq. (13)}$$

The same exercise has been carried out for the other stresses and for the three displacements, for the types of nuclei used in the forward model.

### 4.6 Accuracy of the Approximation with Area Sources

As already indicated in the previous Section, we have chosen not to integrate over the height of a grid block. Instead, the integration over the vertical dimension has been approximated by an evaluation of the function in the centre of the grid block and a multiplication of the result with the value of the reservoir height. We had a number of reasons for this approach. The first reason is that the vertical integration interval is small compared to the horizontal dimensions of the gridblocks and the reservoir. In addition, we did not expect a large impact of the approximation on the lateral variation of the influence functions. Finally, an explicit integration would entail a

---

## Quick Screening Subsidence Calculation

---

significant increase in complexity of the code since the influence function is determined for a compacting source at a fixed depth.

For the validation of the approximation we have taken a square gridblock with an aspect ratio of 0.1 [length, width and height being 200, 200, and 20 m and centred in the origin (0, 0, 0)]. For smaller aspect ratios, the approximation will be better. The only nucleus of strain that needs to be investigated is the centre of compression, since the other types are used as auxiliary nuclei only for use in the construction of the solution.

Figure 3 shows the vertical displacement as a function of vertical position, through the centre of the grid block. When the 3-dimensional integral is evaluated, the resulting displacement in the grid interior changes linearly between the bottom and the top of the gridblock. For the area source, there is a jump in the displacement at the source plane. This behaviour for the two approaches is as expected. What is more interesting is the accuracy of the approximation outside the grid block. From the numerical results we conclude that the mismatch increases to approximately 0.25% at a distance of the order of the lateral size of the block.

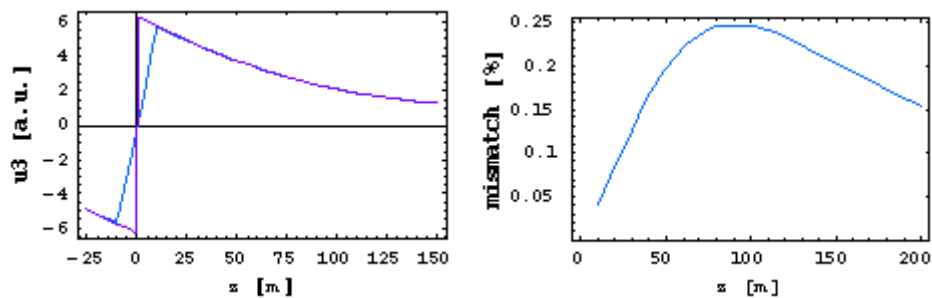


Figure 3 Left: Vertical displacements for volume source and area source along a vertical line through  $(x, y) = (0, 0)$ . Right: Relative differences, outside the gridblock, between results of vertical displacements for a volume source and an area source. The black lines indicate the vertical extent of the grid block.

A same kind of analysis has been performed on a vertical line at a lateral position closer to the boundary of the gridblock and on a line beyond the extent of the gridblock [the positions in the horizontal plane were chosen at  $(x, y) = (80, 0)$ , so the distance from the boundary was 10% of the gridblock size]. Here the horizontal displacements are not zero like they are along the vertical line through. The results, along with the relative errors outside the gridblock, are presented in Fig. 4. The largest error at the top of the gridblock is about 1%. The discrepancy increases when approaching the corner of the gridblock. To illustrate this, the results on a vertical line through  $(x, y) = (100, 0)$  are presented in Fig. 5. The error in vertical displacement remains small but the error in horizontal displacement is larger: about 12% on the block edge. This is related to the concentration of horizontal displacement at the edge of the area, as is seen from the shape of the curve near  $z = 0$ . However, one should realize that the abrupt change of pressure at the lateral boundary of a grid block is an approximation as well. Beyond the grid boundary, the error

## Quick Screening Subsidence Calculation

decreases again [(x, y) = (120, 0); Fig. 6]. The large relative error for the vertical displacement is related to the vanishing displacement at centre depth.

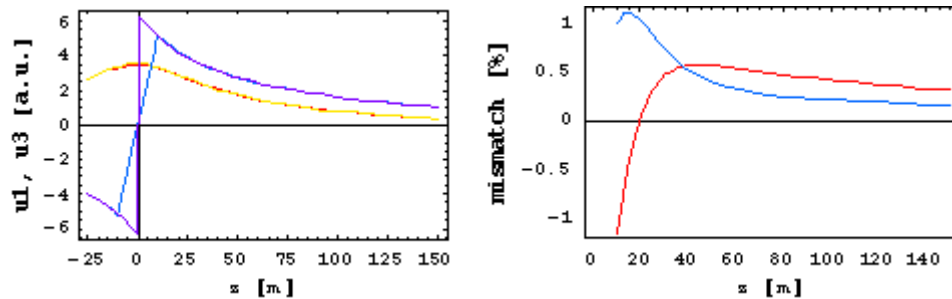


Figure 4 Displacement along a vertical line through (80, 0), inside the block, close to the block edge. Left: Vertical (blue, purple) and horizontal (red, yellow) displacements for volume source and area source. Right: relative differences between results outside the gridblock for a volume source and an area source. Blue for vertical displacements, red for horizontal displacements.

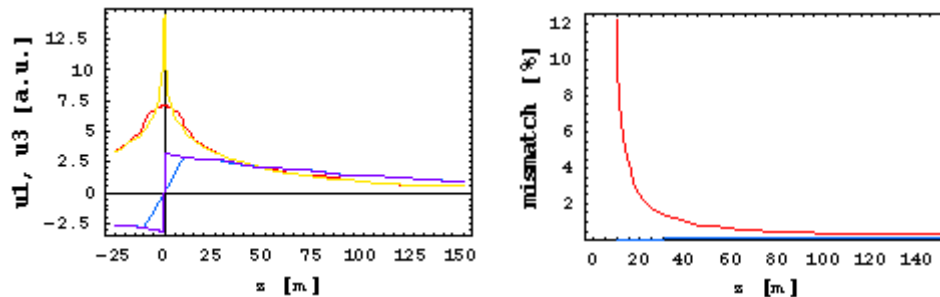


Figure 5 Displacement along a vertical line through (100, 0) at the block edge. Left: Vertical (blue, purple) and horizontal (red, yellow) displacements for volume source and area source. Right: relative differences between results for a volume source and an area source. Blue for vertical displacements, red for horizontal displacements.

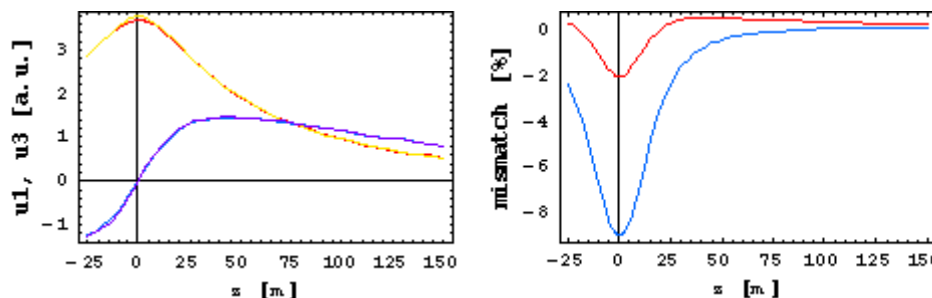


Figure 6 Displacement along a vertical line through (120, 0) outside the block. Left: Vertical (blue, purple) and horizontal (red, yellow) displacements for volume source and area source. Right: relative differences between results for a volume source and an area source. Blue for vertical displacements, red for horizontal displacements.

Even more important than the displacement is the stress, since it is the shear stress that causes reactivation of faults. We have thus performed the same exercise for the stresses. The results are presented in Figs. 7 – 10. Above the centre of the square grid block (Fig. 7) no shear stresses can exist because of the symmetry, and the two horizontal stresses are identical. The Figure shows

## Quick Screening Subsidence Calculation

very good agreement between the area source approach and the volume source, even in the interior of the grid block. Close to the boundary of the grid block (Fig. 8), the normal stresses are still in reasonable agreement. Outside the gridblock ( $z$  larger than 0.1) they do not differ more than a few percent. The shear stress, however, of which only the  $xz$  component is nonzero on in the  $y=0$  plane, shows larger differences: 14% at the boundary [in the point (80, 0, 10)]. The same observations can be made for the results just beyond the boundary of the grid block (Fig. 9). Further away from the boundary the differences fade away quickly. Figure 10, at the centre of the next gridblock  $[(x, y) = (200, 0)]$  shows that the differences have decreased to typically less than a percent. For completeness, we show in Fig. 11 the stresses at the edge of the gridblock. Here the shear stresses are very large.

We conclude that the stresses calculated with area sources and with volume sources agree to an acceptable level. The largest differences are seen near the edge of the grid block and when the actual stresses vanish. For a reservoir simulation with large pressure differences between neighbouring gridblocks the discrepancy between the methods is the consequence of the stepwise changes in pressures. But even then, the difference quickly decreases to less than 10% once the distance to the upper boundary of the gridblock is more than 50% of its height. The approximations become better for smaller aspect ratios: an additional sensitivity analysis revealed that the relative mismatch is proportional to the ratio of the grid block height and its area.

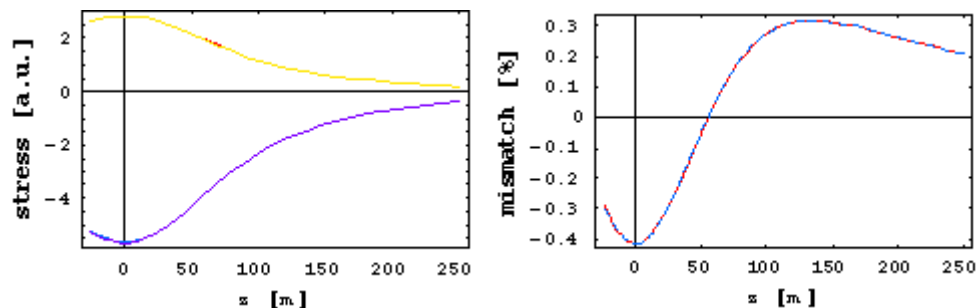


Figure 7 Stresses along a vertical line through  $[(x, y) = (0, 0)]$ . Left:  $\sigma_{11}$  (red, yellow) and  $\sigma_{33}$  (blue, purple) for the volume source and the area source. Right: Relative differences between volume source calculation and area source calculation.

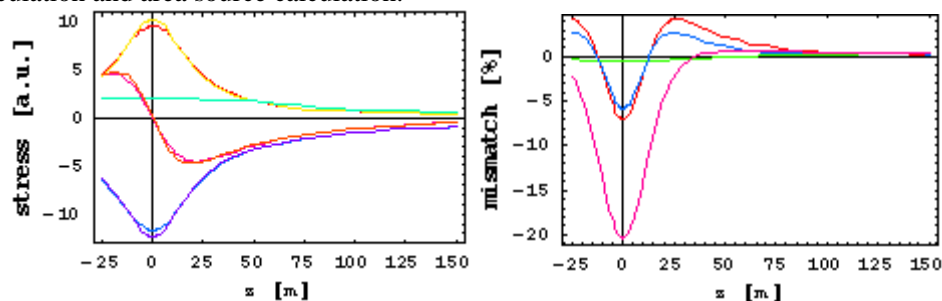


Figure 8 Stresses along a vertical line through  $[(x, y) = (80, 0)]$ , crossing the gridblock. Left:  $\sigma_{11}$  (red, yellow)  $\sigma_{22}$  (green, light green),  $\sigma_{33}$  (blue, purple) and  $\sigma_{13}$  (pink, red) for the volume source and the area

# Quick Screening Subsidence Calculation

source. Right: Relative differences between volume source calculation and area source calculation [ $\sigma_{11}$ : red,  $\sigma_{22}$ : green,  $\sigma_{33}$ : blue, and  $\sigma_{13}$ : pink].

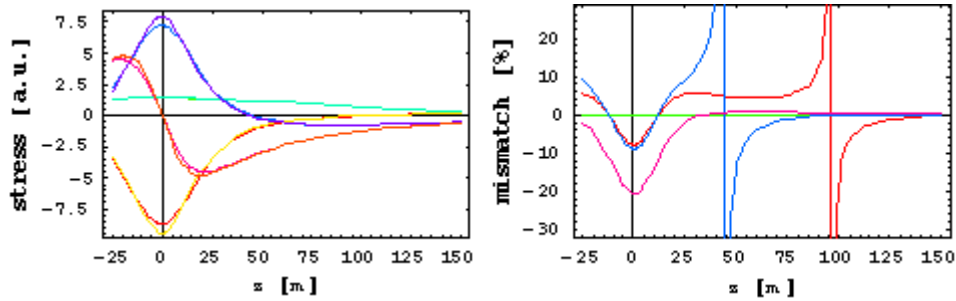


Figure 9 Stresses along a vertical line through  $[(x, y) = (120, 0)]$ , outside the gridblock. Left:  $\sigma_{11}$  (red, yellow)  $\sigma_{22}$  (green, light green),  $\sigma_{33}$  (blue, purple) and  $\sigma_{13}$  (pink, red) for the volume source and the area source. Right: Relative differences between volume source calculation and area source calculation [ $\sigma_{11}$ : red,  $\sigma_{22}$ : green,  $\sigma_{33}$ : blue, and  $\sigma_{13}$ : pink]. The singularities in the right plot are directly related to the zero values of the stresses in the left plot.

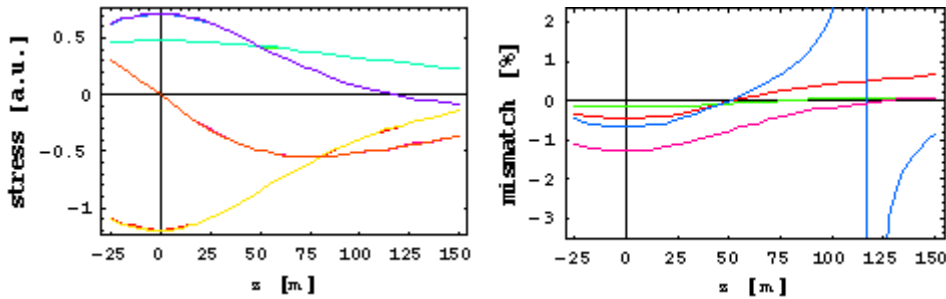


Figure 10 Stresses along a vertical line through  $[(x, y) = (200, 0)]$ , at the centre of the next gridblock. Left:  $\sigma_{11}$  (red, yellow)  $\sigma_{22}$  (green, light green),  $\sigma_{33}$  (blue, purple) and  $\sigma_{13}$  (pink, red) for the volume source and the area source. Right: Relative differences between volume source calculation and area source calculation [ $\sigma_{11}$ : red,  $\sigma_{22}$ : green,  $\sigma_{33}$ : blue, and  $\sigma_{13}$ : pink].

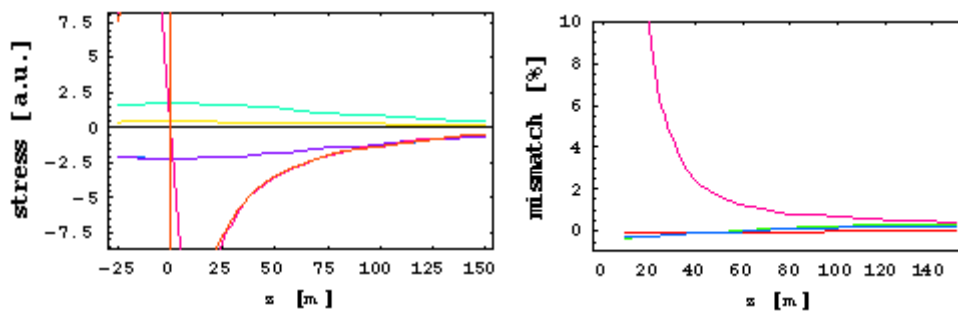


Figure 11 Stresses along a vertical line through  $[(x, y) = (100, 0)]$ , at the edge of the gridblock. Left:  $\sigma_{11}$  (red, yellow)  $\sigma_{22}$  (green, light green),  $\sigma_{33}$  (blue, purple) and  $\sigma_{13}$  (pink, red) for the volume source and the area source. Right: Relative differences between volume source calculation and area source calculation [ $\sigma_{11}$ : red,  $\sigma_{22}$ : green,  $\sigma_{33}$ : blue, and  $\sigma_{13}$ : pink].

## 4.7 Limitations

## Quick Screening Subsidence Calculation

---

The assessment of quality and robustness of the software was described above. 8 to 10 pairs of nuclei are usually sufficient to obtain accurate results for the nucleus-of-strain solution. The auxiliary nuclei must be spaced around the distance of the associated interface to the compacting source in the reservoir. A logarithmic spacing ranging from 0.3 to 8 times that distance usually gives good results. We implemented a default of 13 nuclei with spacing ranging from 0.25 to 13.

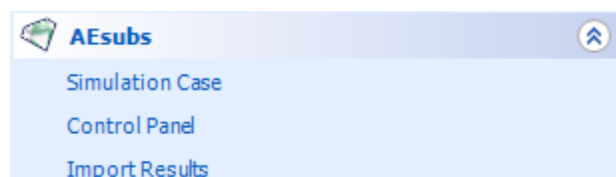
Instabilities have been observed when the elasticity contrast at a layer interface is large, i.e. larger than a factor 10. Large differences in layer thicknesses, or a short distance between the compacting source and one of the interfaces, can also result in instabilities. It is therefore advisable to always check the quality of the approximation before proceeding with the integration exercise.

The compaction field of a reservoir can not always be given in a regular grid with all the same areal source at every location. It is therefore still possible to input the compaction grid in a so-called  $x$ - $y$ - $c$  file format: a finite amount  $c$  of compaction is concentrated at the field depth at the lateral position  $(x,y)$ . For such point sources, the resulting displacements, stresses, and strains may be inaccurate when the point of their calculation is closer than 10 times the real extent of the source. That is to say, if the distance is larger than 10 times the extent of a grid block, the approximation of the grid block by a point source usually results in an error of less than 1%. This possible inaccuracy is the reason that the software gives the user a warning when he wants to make calculations on a user-defined line or plane when the compaction input is in point sources.

The software uses area sources instead of volume sources; it concentrates the full height of the reservoir at a single depth. We have earlier discussed [1] that the stresses calculated with area sources and with volume sources agree to an acceptable level. The largest differences are seen near the edge of the grid block and when the actual stresses vanish. For a reservoir simulation with large pressure differences between neighbouring gridblocks the discrepancy between the methods is the consequence of the stepwise changes in pressures. But even then, the difference quickly decreases to less than 10% once the distance to the upper boundary of the gridblock is more than 50% of its height. The approximations become better for smaller aspect ratios: an additional sensitivity analysis revealed that the relative mismatch is proportional to the ratio of the grid block height and its area.

## 5 JewelSuite integration

AESubs is seamlessly integrated in the GUI of JewelSuite. The 3D geological models build in JewelSuite, can be used directly as an input for AESubs. Also, other input parameters that



# Quick Screening Subsidence Calculation

need to be defined for AESubs, can be set within the JewelSuite environment.

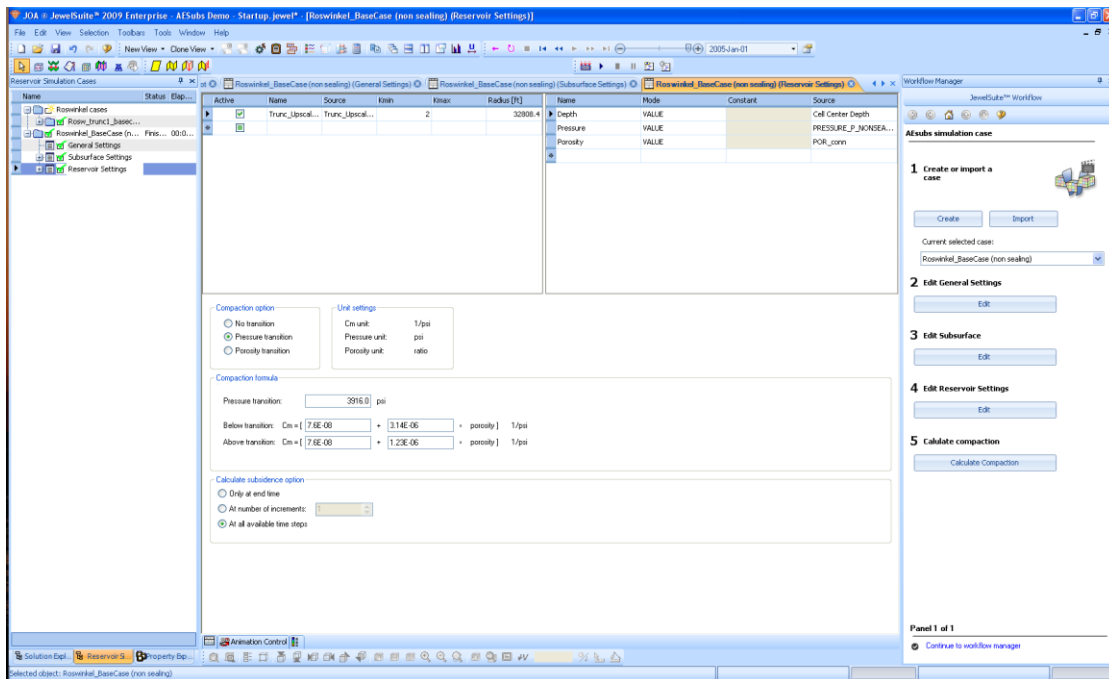


Figure 12: Input parameters for AESubs are specified from within the JewelSuite user interface

Once calculations in AESubs are finished, the results are sent back to JewelSuite for further analysis. The results can be analyzed, either graphically in the 3D view in conjunction with the original 3D geological model, or using XY plots, to display parameters as 'maximum subsidence', 'bowl volume' and 'nucleus'.

# Quick Screening Subsidence Calculation

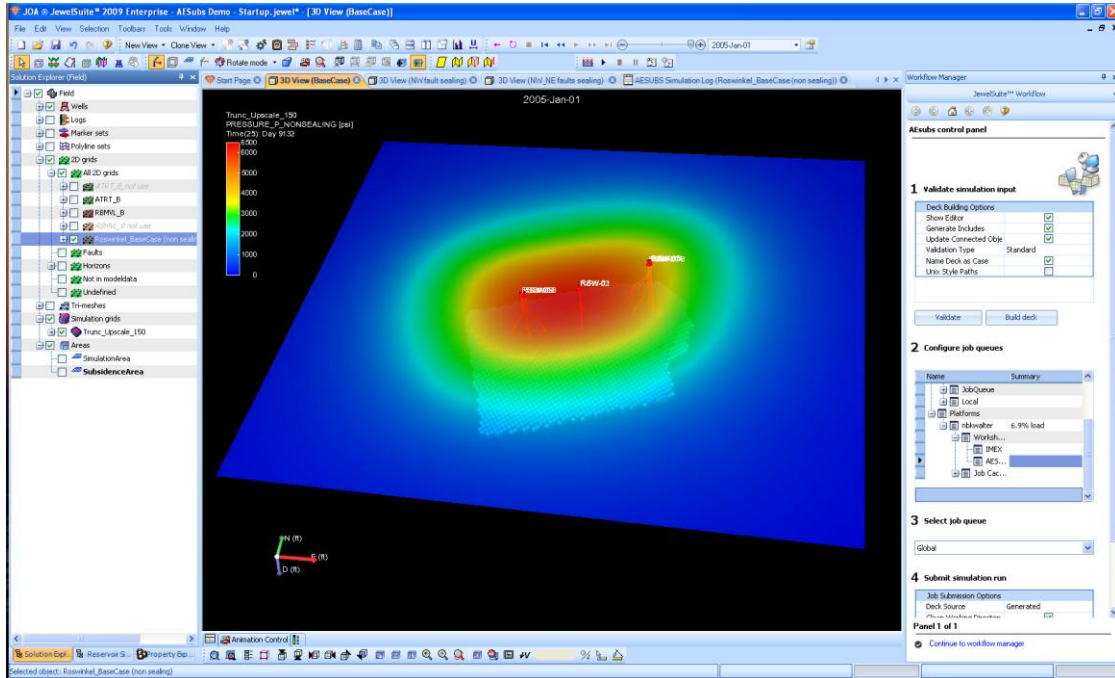


Figure 13: Visualization of Subsidence bowl with geological grid underneath

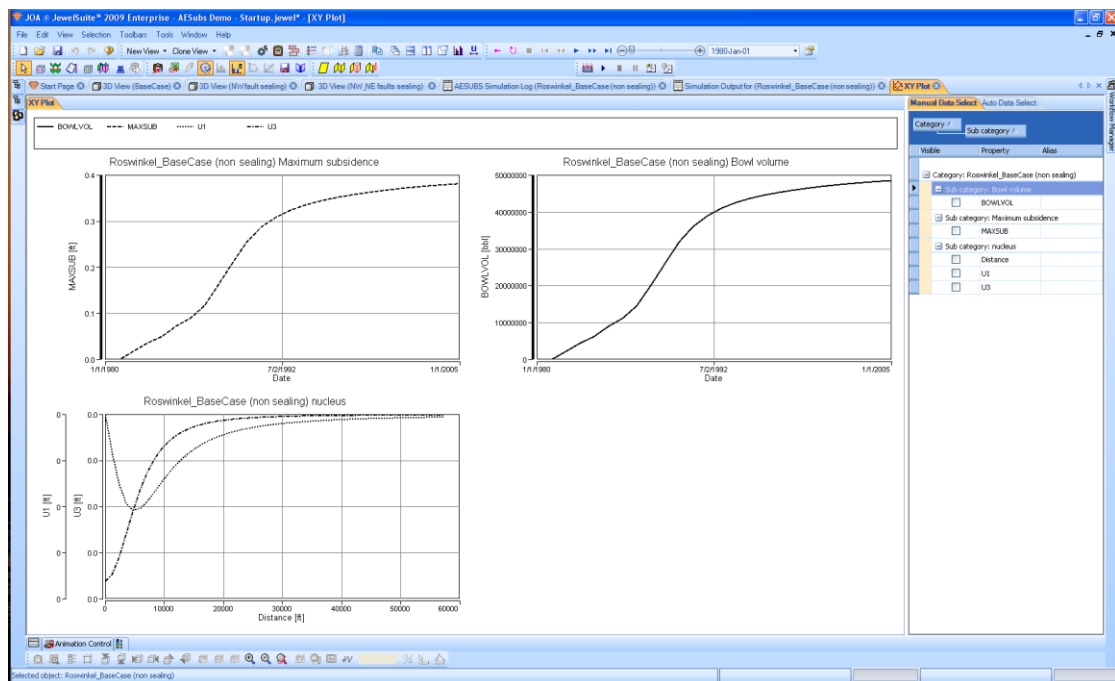


Figure 14: XY plots of Maximum subsidence, Bowl volume and Nucleus (U1 & U3)